RSC Advances

PAPER

View Article Online
View Journal | View Issue

Cite this: *RSC Adv.*, 2026, **16**, 27180

Histidine-conjugated chitosan as efficient adsorbent for Congo red dye elimination from aqueous solution

Jawza Sh Alnawmasi, Nouf F. Al-Harby, * Azizah A. Algreiby, Tahani Alresheedi and Nadia A. Mohamed *

Received 4th March 2026
Accepted 11th May 2026

DOI: 10.1039/d6ra01879c

rsc.li/rsc-advances

A two-step procedure was employed to synthesize histidine-conjugated chitosan (His–Cs). Initially L-histidine (His) was reacted with epichlorohydrin in an alkaline medium, followed by reaction of the resultant product with chitosan (Cs) in the same medium, producing His–Cs (yield = 96.5%). The chemical structure of His–Cs was verified using suitable analytical methods, including FTIR, XRD, SEM, and EDS. His–Cs was utilized as an adsorbent and demonstrated exceptional capabilities for the adsorption of Congo Red (CR) dye. The equilibrium results aligned with the Temkin adsorption isotherm. The greatest removal efficiency of His–Cs for CR dye was 99.17%. The Elovich model precisely described the kinetics of adsorption. The adsorption process was endothermic at the applied temperatures. The results indicate that His–Cs may be effectively utilized for the extraction of CR dye from aqueous solutions.

1. Introduction

Water contamination with synthetic dyes poses a significant hazard to humans and aquatic organisms.[1–3] Water is polluted by discharging effluents containing synthetic dyes from industries such as textile, cosmetic, leather, plastic, paper, photography, medicinal drugs, and food.[4] Very small quantities of these dyes in water were found to cause a noticeable and non-acceptable impact such as undesirable coloration of the water, obstruction of light and oxygen from accessing aquatic creatures, along with significant harm to the liver, digestive, and central neurological systems in humans.[5] This is due to their toxicity, and non-biodegradability resulted from their complicated structure and high stability against heat and light.[6–8] Among the synthetic dyes particularly, is the diazo anionic dye, 1-naphthalene sulfonic acid, 3,3′(4,4′biphenylenebis(azo))bis(4-amino-)disodium salt, or the so-called Congo Red (CR) dye, that has demonstrated considerable concern due to its carcinogenic benzidine moiety, high stability, and high toxicity.[9–11] In spite of prohibition of its use in many countries, it is yet vastly utilized in textile industry in other numerous ones nowadays. In this regard, the removal of CR dye remainders from the effluents before discharge into the environment is one of the major global environment attentions. For this, numerous techniques were employed such as ultrafiltration,[12] reverse osmosis,[13] ozone treatment,[14] oxidation,[15] flocculation/coagulation,[16] ion exchange,[17] and photo catalytic degradation.[18] Although these methods are all effective but they have disadvantages and limitations such as high cost, high energy consumption, undesirable/toxic by-products, and poor performance at low dye concentrations. For the time being, the adsorption technique is deemed to be one of the most competitive ways to the aforementioned traditional methods. This is attributed to its high efficiency, operational simplicity, rapid processing, ease of handling, low initial cost, wide availability of adsorbent materials, lack of harmful secondary byproducts, and the straightforward regeneration of adsorbents for reuse.[19] Thus, it became of interest to direct the present study to synthesize a modified non-conventional polycationic bio-adsorbent based on a naturalistic matter, chitosan, and evaluate its adsorption performance to remove the anionic CR dye from its aqueous solution.

Chitin, a natural biopolymer, ranks as the second most abundant polysaccharide following cellulose. It is derived from the exoskeleton of cartilages of crustaceans, cell walls of microorganisms, mollusks, and insects. The deacetylation of chitin produces the biopolymer Cs which is made up of 2-amino-2-deoxy-β-D-glucopyranose and 2-acetamido-2-deoxy-β-D-glucopyranose bonded by β(1,4)-linkage.[20] Cs, similar to the other natural biopolymers, possesses some unique properties such as non-toxicity, bulk availability, renewability, hydrophilicity, antimicrobial activity, biodegradability, and biocompatibility. It has polycationic chains that can effectively bind with the negatively charged species, allowing its usage in water treatment domains to get rid the anionic pollutants.[21] The utilization of Cs as an adsorbent is constrained by its high solubility and limited structural stability in acidic media, low mechanical strength, low surface area, low thermal resistance and low porosity. These shortcomings represent hindrances facing a lot of its applications especially its usages to adsorb dyes since

Department of Chemistry, College of Science, Qassim University, Buraidah 51452, Saudi Arabia. E-mail: hrbien@qu.edu.sa; NA.AHMED@qu.edu.sa

their effluents are generally acidic. To overcome these disadvantages, a chemical modification of Cs should be performed by either formation of its derivatives,[22] grafting copolymerization,[23,24] blending with other polymer,[25,26] or crosslinking.[27–29] These modifications improve the Cs features *via* incorporating a wide variety of additional functional groups, decreasing its solubility and enhancing its resistance to degradation in acidic media, and reinforcing its articles life span in various solutions.

His is an essential amino acid characterized by the presence of an α-amino group, a carboxylic group, and an imidazole functional group as a side chain. Under acidic conditions, it is classified as a positively charged amino acid due to the protonation of both its amino group and imidazole ring. Functionalization of Cs with His for improvement of its metal binding efficiency was extensively studied.[30–33] Also, His was incorporated into Cs to enhance the gene transfection efficiency,[34] to improve the oral delivery system for insulin,[35] to sustain drug delivery,[36] and to efficiently carry doxorubicin.[37]

Despite of the large number of reported scientific publications concerning modification of Cs to fabricate a vast number of adsorbents,[22–29] there is no works published the application of His–Cs as an adsorbent to remove dyes from aqueous solution for industrial wastewater remediation. Thus, the current study addresses the limitations of Cs and improves its adsorption capabilities for CR dye from aqueous solutions to remediate industrial wastewater by incorporating His moieties as pendant groups on the Cs chains. This was achieved by targeting the lone pair of electrons on the nitrogen in the amino group of His to cleave the epoxide moieties of epichlorohydrin. The resultant product was further condensed with Cs by removal of HCl, yielding His–Cs. The chemical structure of the latter was confirmed by appropriate analytical methods, including FTIR, XRD, SEM, and EDS investigations. The integration of nitrogen-rich His moieties as pendant groups on the Cs backbone repeat units, together with the residual functional groups on Cs will increase the number of available basic sites, thereby enhancing its ability to adsorb the anionic CR dye. The adsorption process was evaluated by investigating various parameters such as solution pH, initial dye concentration, temperature, ionic strength of the solution, and contact time, with the aim of determining the optimal conditions for maximizing adsorption capacity. In addition, the kinetic, and isotherm of the adsorption process were investigated. The thermodynamic parameters (entropy, enthalpy, and the free energy of adsorption) were determined. The possibility of regeneration of the His–Cs for reuse was also studied.

2. Materials and methods

2.1. Materials

Cs (molecular weight = 1.0–3.0 × 10^5 g mol^{-1}, and degree of deacetylation = 98%) was purchased from Acros Organics (USA). Epichlorohydrin was obtained from Panreac. AppliChem-ITW Reagent (Germany). His was supplied by Sigma-Aldrich (Germany). CR dye (Fig. 1) was provided by Winlab (UK). The solvents and other chemicals were purchased from Aldrich (Germany).

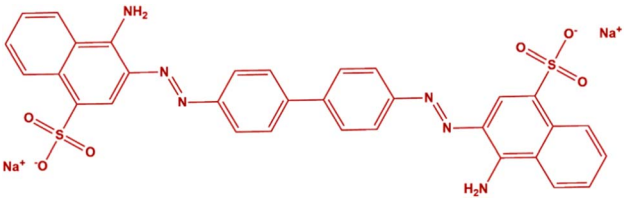

Fig. 1 Chemical structure of CR dye.

2.2. Methods

2.2.1. Synthesis of His–Cs adsorbent. His–Cs was prepared according to the procedure described previously with a slight modification[33] as shown in Scheme 1. His (3.1 g, 0.02 mol) was suspended in aqueous NaOH solution (100 mL, 0.1 M) and stirred at 60 °C for 15 min. To this suspension, epichlorohydrin (1.9 mL, 0.02 mol) was added and stirred at 60 °C for 4 h. The resulting reaction mixture was added to Cs (3.24 g, 0.02 mol), that was swollen in aqueous NaOH solution (100 mL, 0.1 M) at 60 °C for 15 min, and stirred at 60 °C for 8 h. The reaction medium was cooled, neutralized to pH 7 using aqueous acetic acid solution (10% v/v). Then, aqueous MeOH (70% v/v) was added till complete precipitation. The resulting precipitate (His–Cs) was separated by filtration, sequentially washed with distilled water, methanol, and acetone, and then dried at 60 °C until a constant weight (yield: 96.5%, appearance: coarse powder, and color: pale yellow) was achieved.

2.3. Analysis

2.3.1. FTIR spectroscopy. A Cary 600 Series Agilent Technologies FTIR Spectrometer (USA) was employed for recording FTIR spectra of the His–Cs and its components (Cs, and His) from 4000 to 500 cm^{-1} wavenumber range.

2.3.2. X-ray diffractometry (XRD). A Rigaku Ultima-IV Wide-angle X-ray Diffractometer (Japan) was employed to investigate the inner structure of His–Cs and its components (Cs, and His) at diffraction angles (2θ) ranging from 5° to 90° with a scanning speed of 5° min^{-1}.

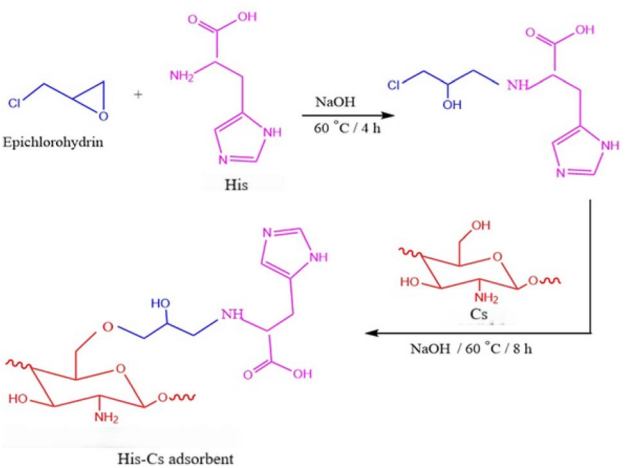

Scheme 1 Preparation of His–Cs adsorbent.

2.3.3. Scanning electron microscopy (SEM). SEM images of the surface topography of His–Cs and Cs, that have been coated with a thin gold layer, were obtained using Field Emission Scanning Electron Microscope JSM-7610F (Jeol, Freising, Germany) provided with an Energy Dispersive X-ray Spectrometer (EDS).

2.3.4. pH value of zero-point charge (pH_{zpc}). The His–Cs adsorbent (100 mg) was soaked in aqueous solution of sodium chloride (10 mL, 0.1 M concentration) overnight. Thereafter, aqueous solutions of hydrochloric acid and sodium hydroxide (0.1 N concentration) were employed for adjusting the pH values to be between 3 and 12, which were measured using a pH meter (Hanna Model 211, Padova, Italy). The value of the pH_{zpc} was procured from the plot of the initial pH *versus* the ΔpH (final pH − initial pH).

2.4. Adsorption studies

The adsorption studies of CR dye using His–Cs adsorbent were conducted *via* batch technique. Typically, 10 mg of His–Cs was added to 10 mL of 100 ppm CR dye solution in an Erlenmeyer flask and allowed to stand for 24 h. The concentration of CR dye was assessed using Shimadzu UV-Vis 1601 spectrophotometer, Japan, at 497 nm (maximum absorbance wavelength of CR dye, Fig. 2). The adsorption capacity and % removal efficiency of His–Cs were determined using eqn (1)–(3).

$$q_e = (C_0 - C_e)(V/m) \quad (1)$$

$$q_t = (C_0 - C_t)(V/m) \quad (2)$$

$$\%\ \text{Removal efficiency} = \frac{(C_0 - C_e)}{C_0} \times 100 \quad (3)$$

where C_0, C_e, and C_t (mg L^{-1}) are the concentration of the solution of CR dye prior and after adsorption (at equilibrium time, and time t), respectively, V (mL) is the volume of the solution of CR dye, m (g) is the mass of His–Cs, q_e and q_t (mg g^{-1}) is the adsorption capacity at equilibrium time and time t, respectively.

The optimal values were ascertained through the analysis of pH (3–9), starting concentration of CR dye (40–200 ppm), and temperature (25–55 °C) using a batch approach. To conduct the adsorption kinetics, 50 mL of CR dye solution with a known concentration of 40 ppm was treated with 50 mg of His–Cs at a specified pH for the defined length of contact (5–2640 min). Adsorption isotherm tests were conducted by treating 10 mg of His–Cs with 10 mL of CR dye solution at varying concentrations from 40 to 200 ppm, at pH 5.5 for 24 h at 25 °C. Each experiment was carried out in (at least) duplicate.

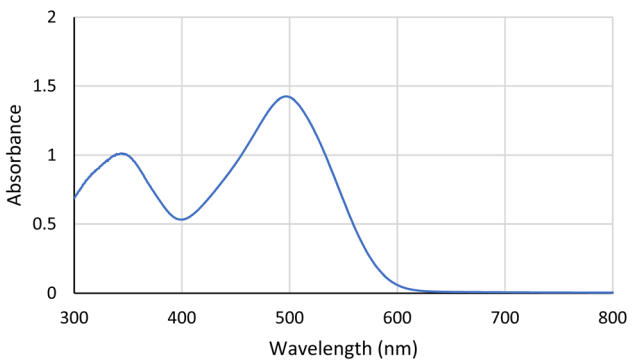

Fig. 2 UV-Vis absorbance of CR dye (pH = 5.5).

2.4.1. Adsorption kinetic studies. The investigation of adsorption kinetics is fundamental to elucidating the rate-limiting steps governing adsorbate interaction with the particle surface, providing critical insight into the influence of physicochemical variables on the overall adsorption dynamics. This approach involves the application of kinetic models that precisely characterize the system's response, thereby enabling a detailed interpretation of the underlying mechanism through which dye molecules are adsorbed onto the surface of the adsorbent material.[38]

The adsorption kinetics of CR dye were examined by fitting the data to three separate kinetic models; pseudo first order, pseudo second order, and Elovich (Table 1).

2.4.2. Investigation of adsorption isotherms. The adsorption isotherm serves as a fundamental tool for understanding the surface properties and behavior of the adsorbent material. Selecting the appropriate adsorption model across different concentration ranges enables a comprehensive understanding of the adsorbent surface characteristics. The adsorption isotherm provides insight into several key aspects, including the equilibrium distribution of adsorbate molecules between the liquid and solid phases, the nature of the interactions between the adsorbate and the adsorbent, and the classification and characteristics of the adsorption process. The adsorption system was characterized by fitting the data to various models, including Freundlich, Langmuir, and Temkin models (Table 2).[40]

2.5. Thermodynamic study

Study of the adsorption thermodynamic contributes to determine the feasibility and direction of this process. *Via* this study, some significant parameters can be obtained, including Gibbs free energy ($\Delta G°$, kJ mol^{-1}), enthalpy change ($\Delta H°$, kJ mol^{-1}) and entropy change ($\Delta S°$, J mol^{-1} K^{-1}). These parameters were calculated at different temperatures (298, 308, 318 and 328 K) in accord to eqn (4) and (5).[7]

$$\Delta G^\circ = -RT \ln K_c \quad (4)$$

$$\ln K_c = \frac{\Delta S^\circ}{R} - \frac{\Delta H^\circ}{RT} \quad (5)$$

where R (8.314 J mol^{-1} K^{-1}) is the universal gas constant, $K_c(q_e/C_e)$ is the equilibrium constant and T (K) is the absolute temperature. The thermodynamic parameters can be calculated from the plot of ln K_c *versus* $1/T$.

2.6. Reusability study

The regeneration of His–Cs was evaluated through repeated adsorption–desorption cycles. Briefly, 0.01 g of His–Cs was immersed in 10 mL of CR dye solution (40 ppm) and

Table 1 List of the common kinetic models.[39]

Kinetic model	Non-linear form	
Pseudo first order	$q_t = q_e e^{-k_1 t}$	k_1 (min^{-1}) is the pseudo first order rate constant
Pseudo second order	$q_t = \frac{k_2 q_e^2 t}{1 + k_2 q_e t}$	k_2 (g mg^{-1} min^{-1}) is the pseudo second order constant
Elovich	$q_t = \frac{1}{\beta} \ln(\alpha\beta) + \frac{1}{\beta} \ln t$	β (g mg^{-1}) represents the rate constant, often referred to as the desorption constant, which is associated with the activation energy of chemisorption and the extent of surface coverage, and α (mg g^{-1} min^{-1}) denotes the initial adsorption rate constant, indicating the starting rate of the adsorption process

Table 2 List of the common isotherm models[41]

Isotherm model	Non-linear form	
Langmuir	$q_e = \frac{q_{max} K_L C_e}{1 + C_e K_L}$	q_{max} (mg g^{-1}) indicates the maximum adsorption capacity corresponding to the monolayer coverage, K_L (L mg^{-1}) is a constant associated with the adsorption energy, and R_L represents the Langmuir separation factor, a dimensionless parameter that characterize the nature of the isotherm
	$R_L = \frac{1}{(1 + K_L C_0)}$	The isotherm can be classified as linear ($R_L = 1$), unfavorable ($R_L > 1$), favorable ($0 < R_L < 1$), and irreversible ($R_L = 0$)
Freundlich	$q_e = K_F C_e^{n_F}$	K_F (mg g^{-1}) (L mg^{-1})$^{1/n}$ and n are empirical parameters that correspond to the adsorption capacity and adsorption intensity, respectively
Temkin	$q_e = \frac{RT}{B_T} \ln K_T C_e$	B_T (J mol^{-1}) is the Temkin constant related to the influence of temperature on the adsorption process, and K_T (L g^{-1}) represents the Temkin isotherm binding constant[42,43]

maintained for 24 h to allow adsorption equilibrium. After recovery of the adsorbent, desorption was carried out by treating the material with 0.1 M HCl solution for 24 h to elute the retained dye molecules. The regenerated His–Cs was then thoroughly washed with deionized water to remove any residual acid prior to reuse. The adsorption–desorption procedure was repeated for three consecutive cycles under identical operating conditions using the same adsorbent sample.[44]

3. Results and discussion

3.1. FTIR spectroscopy

Fig. 3 presents the FTIR spectrum of Cs prior and after modification with His. In pristine Cs, a wide peak was noticed in the range from 3600 to 3100 cm^{-1}, attributed to stretching vibrations of both the overlapped hydrogen bonded OH and NH_2 groups. The two weak peaks at 1650 and 1562 cm^{-1} correspond to amide I and amide II, respectively, emphasizing the great extent of deacetylation of Cs. Further, the appearance of four distinct peaks at 1157, 1072, 1026, and 891 cm^{-1} confirmed the existence of the saccharide units within the Cs structure, as previously reported.[45]

His exhibited characteristic FTIR absorption bands, including a broad range at 3300–2500 cm^{-1} attributed to the overlapping stretching vibrations of NH_2 and OH group of the carboxylic group $\left(\mathrm{CO\underline{OH}}\right)$, along with CH stretching (Fig. 3). A peak at 1735 cm^{-1} corresponded to the $\underline{\mathrm{CO}}$OH stretching. The stretching vibration peaks of C=C and C=N in the imidazole ring overlapped with each other, giving one peak that appeared at 1631 cm^{-1}.[33]

FTIR spectrum of His–Cs showed a combination between both the characteristic absorption peaks of its components (Cs and His). The peak of OH and NH of the His moiety overlapped with the corresponding one of the Cs. Also, the peak of C=C and C=N of the imidazole ring of His moiety overlapped with amide I peak of Cs. The appearance of the peak at 1735 cm^{-1}, that corresponded to $\underline{\mathrm{CO}}$OH of His, in addition to the appearance of the peaks of the saccharide units of Cs, indicated the successful incorporation of His moieties into the Cs chains (Fig. 3).

3.2. XRD analysis

XRD was used to investigate the structural evolution of His–Cs relative to its individual components (His and Cs), with equal sample masses. The corresponding diffraction patterns are shown in Fig. 4.

3.2.1. Crystalline structure of His. His exhibited multiple sharp diffraction peaks at 2θ = 9.34°, 15.22°, 18.82°, 21.04°, 24.18°, and 30.92°, confirming its well-defined crystalline nature. These peaks were indexed using the standard reference data for L-histidine from the International Center for Diffraction Data (ICDD, PDF no. 51-2290), corresponding to the orthorhombic polymorph (space group $P2_12_12_1$). The reflections at 9.34°, 15.22°, 18.82°, 21.04°, 24.18°, and 30.92° were assigned to the (001), (010), (020), (110), (111), and (021)/(121) planes, respectively. The most intense peak at 18.82° corresponds to the (020) plane, indicating a preferential crystallographic orientation along this direction.

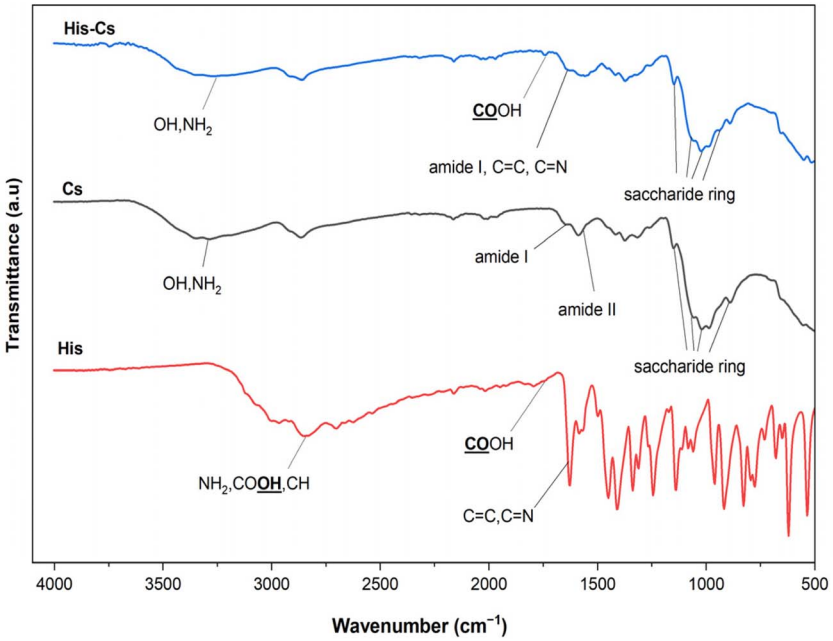

Fig. 3 FTIR spectra of His, Cs, and His–Cs.

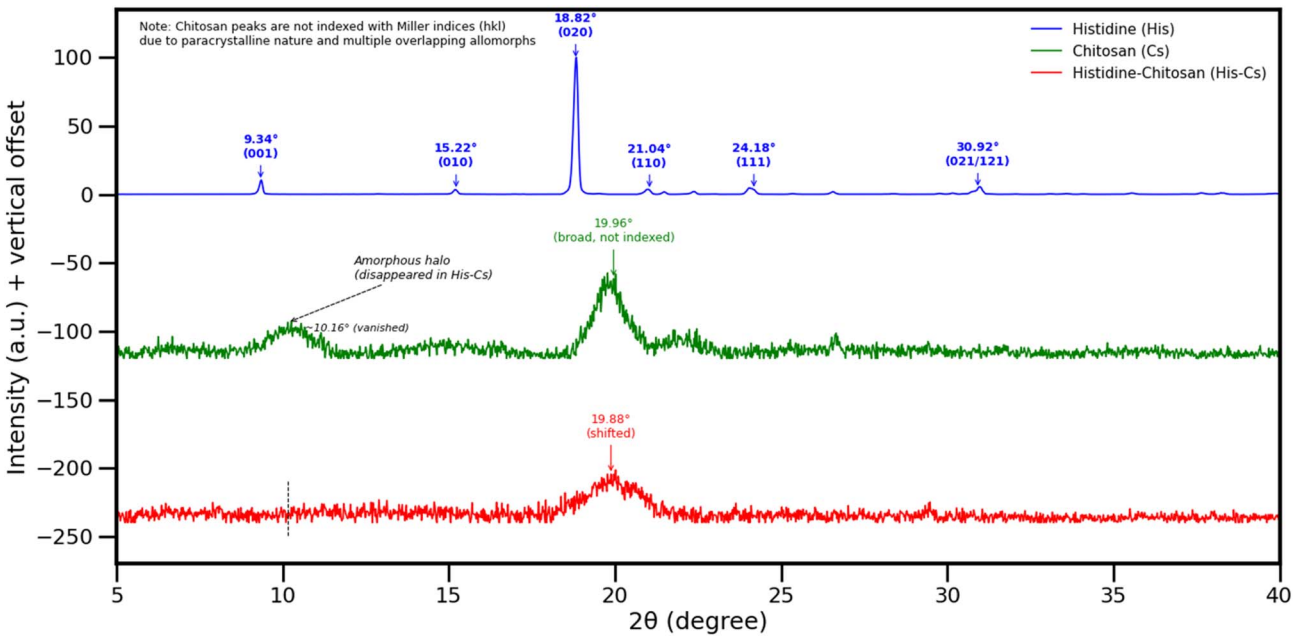

Fig. 4 XRD patterns of His, Cs, and His–Cs.

3.2.2. Semi-crystalline nature of Cs. Pristine Cs exhibited two characteristic broad diffraction features centered at approximately $2\theta = 10.16°$ and 19.96°, indicative of its semi-crystalline nature.[46] The broad halo near 10.16° is typically attributed to amorphous and hydrated domains, whereas the peak near 19.96° corresponds to interchain packing within partially ordered regions. Unlike crystalline His, chitosan cannot be assigned specific Miller indices (*hkl*) because of its paracrystalline nature and the presence of multiple overlapping allomorphs.

3.2.3. Structural evolution of the His–Cs composite. The His–Cs composite showed a noticeable change in the diffraction profile. Specifically, the broad amorphous/hydrated halo originally centered at ~10.16° disappeared, while the main peak shifted slightly from 19.96° to 19.88° and increased in intensity. According to Bragg's law, a shift toward a lower diffraction angle corresponds to a slight increase in interplanar spacing (from 4.44 Å to 4.46 Å), suggesting a reorganized, more compact, and more ordered arrangement within the polymer matrix, due to intermolecular interactions between His and Cs. Weak

contributions from His crystalline domains may also be present but are significantly attenuated, likely due to their molecular-level dispersion within the Cs network.

3.2.4. Mechanism of structural modification. These structural modifications are attributed to the successful incorporation of His moieties into the Cs matrix, which introduces additional intermolecular interactions. In particular, hydrogen bonding between His's imidazole ring and the hydroxyl and amino groups of Cs is proposed to reduce polymer chain mobility and promote a more organized macromolecular arrangement, thereby increasing apparent crystallinity and structural order.

3.3. SEM analysis

The surface topography of the His–Cs was photographed using the scanning electron microscope and its image was shown in Fig. 5. The surface of the pristine Cs seemed almost smooth, while His–Cs showed a gruff surface full of lumps due to incorporated His moieties. There is a homogeneous distribution of these lumps over the His–Cs, indicating the completeness of the modification process of Cs.

Thus, FTIR spectrum, XRD pattern, and SEM image of the His–Cs, in comparison to those of the pristine Cs, greatly affirmed the successful modification process of chitosan. However, elemental composition and distribution of both His–Cs and the pristine Cs was identified using EDS technique, to provide further evidence for the successful preparation of His–Cs. EDS mapping analysis creates detailing the spatial distribution and concentration of elements across a sample's surface, allowing to develop a greater understanding of a sample structure. The results of inspection of elemental composition revealed a perceptible increment in the percentage of both C and N elements on the expense of oxygen element of His–Cs (54.43, 10.04, and 35.53%, respectively) as compared to those of the pristine Cs (51.6, 7.0, and 41.4%, respectively) as shown in Fig. 6. This confirmed the incorporation of His moiety into Cs, supporting the results of the aforementioned techniques utilized for proving the successful synthesis of His–Cs. Further, the distribution maps of carbon, oxygen, and nitrogen elements in the investigated samples appeared homogenous as illustrated in Fig. 6. It is merit mentioning that the degree of substitution of the synthesized His–Cs was found to be 65, that was calculated based on its C/N value using the formula previously reported.[47]

3.4. Adsorption parameters

The adjustment of pH is crucial in adsorption experiments. Therefore, the influence of pH on the adsorption of CR dye by His–Cs was examined across a pH range of 3 to 9, as illustrated in Fig. 7(a).

It was found that the % removal efficiency of CR dye by His–Cs increased with decreasing pH of the medium, *i.e.*, it was 19.1% at pH 9, 79.1% at pH 7, 82.78% at pH 5.5, 85.76% at pH 4, and 96.04% at pH 3. This behavior can be attributed to the pH-dependent ionization of functional groups on the adsorbent surface as well as the electrostatic interactions between the dye molecules and the adsorbent.

At pH 3, most of the oxygen and nitrogen-containing groups on both Cs and His moieties are protonated to form positively charged groups. This results in an adsorbent with highly positive surface charge, leading to strong electrostatic attraction between the adsorbent and the anionic CR dye.

As the pH increases, partial deprotonation of nitrogen-containing groups occurs, reducing the surface's positive charge and thus decreasing electrostatic attraction. In addition, at high pH, both the –OH and –COOH groups were deprotonated to their corresponding anions, inducing a repulsion force with the anionic CR dye. This reduces the accessibility of dye molecules to active sites, resulting in a significant decrease in adsorption.

The pH at which the net surface charge becomes zero under specific solution composition and temperature conditions is referred to as the point of zero charge (pH_{zpc}). This condition does not imply the absence of surface charges; rather, it indicates that the number of positively charged sites equals that of negatively charged sites. The magnitude and nature of the surface charge depend on the abundance and type of surface functional groups, as well as the solution pH. The pH_{zpc} plays

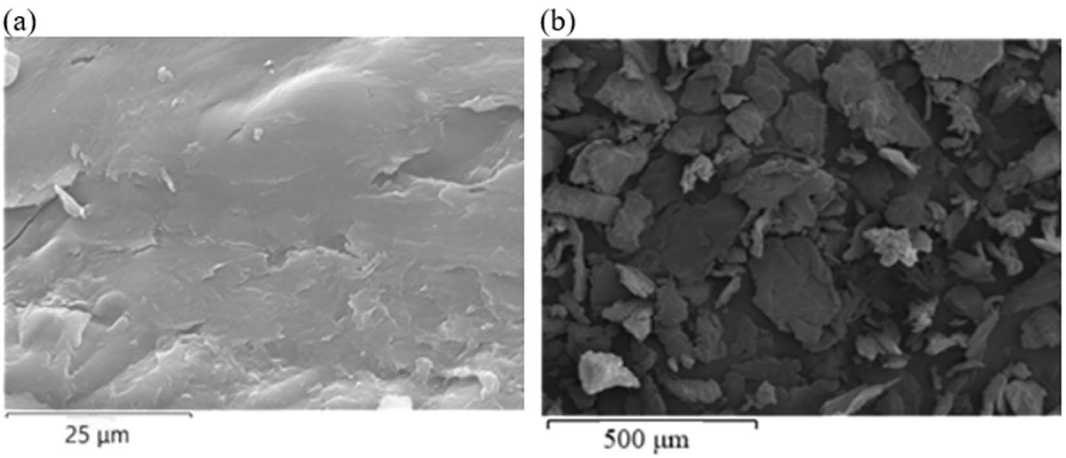

Fig. 5 SEM images of: (a) Cs, and (b) His–Cs. All the gold coated samples were photographed at a magnification of 2500×.

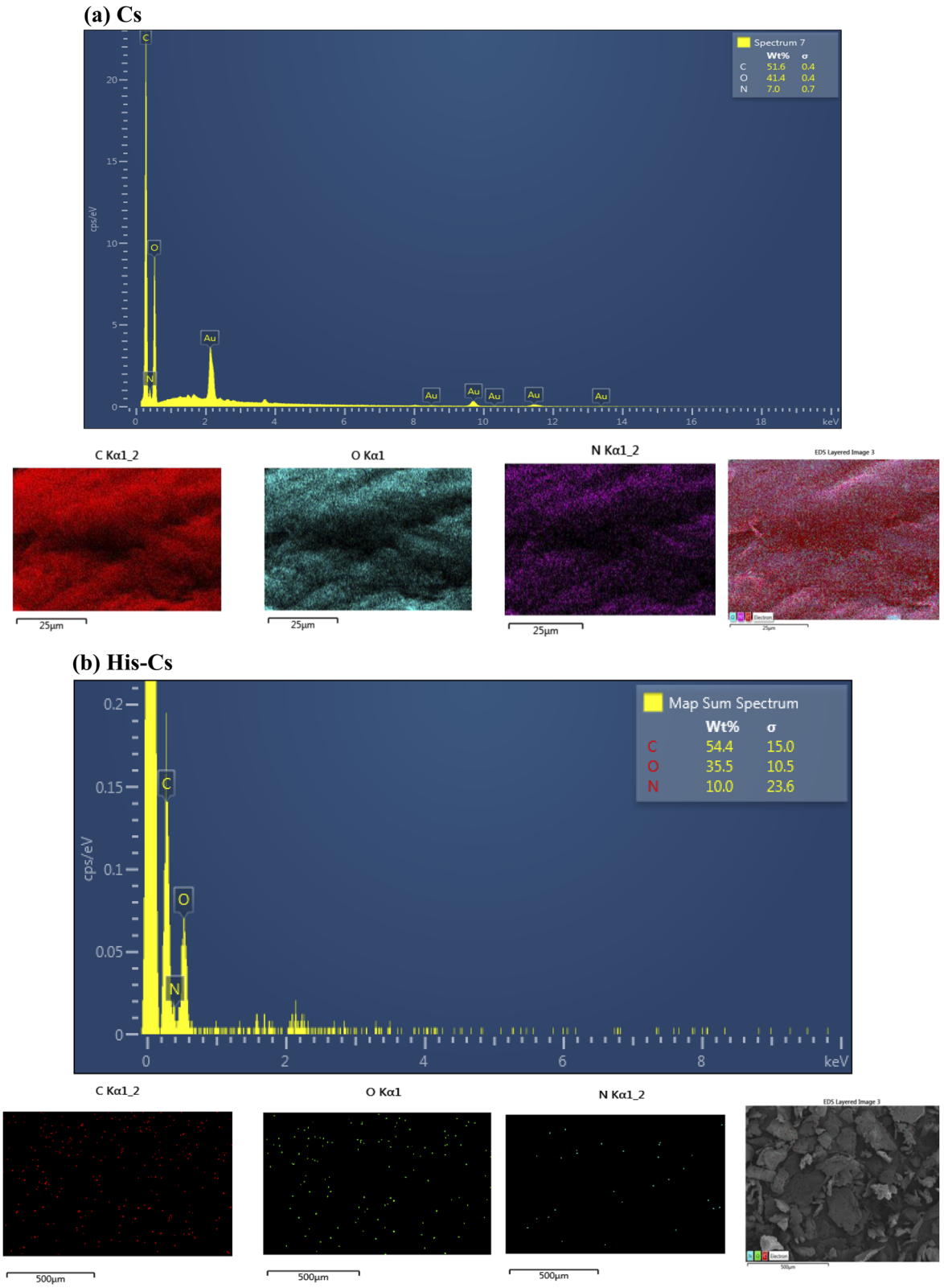

Fig. 6 Concentration and distribution maps of carbon, oxygen, and nitrogen elements of: (a) Cs, (b) His–Cs.

a crucial role in surface characterization because it governs the electrostatic interactions between the adsorbent and ionic species in solution. When the solution pH exceeds the pH_{zpc}, the adsorbent surface acquires a net negative charge, thereby favoring the adsorption of positively charged species. Conversely, at pH values below the pH_{zpc}, the surface becomes

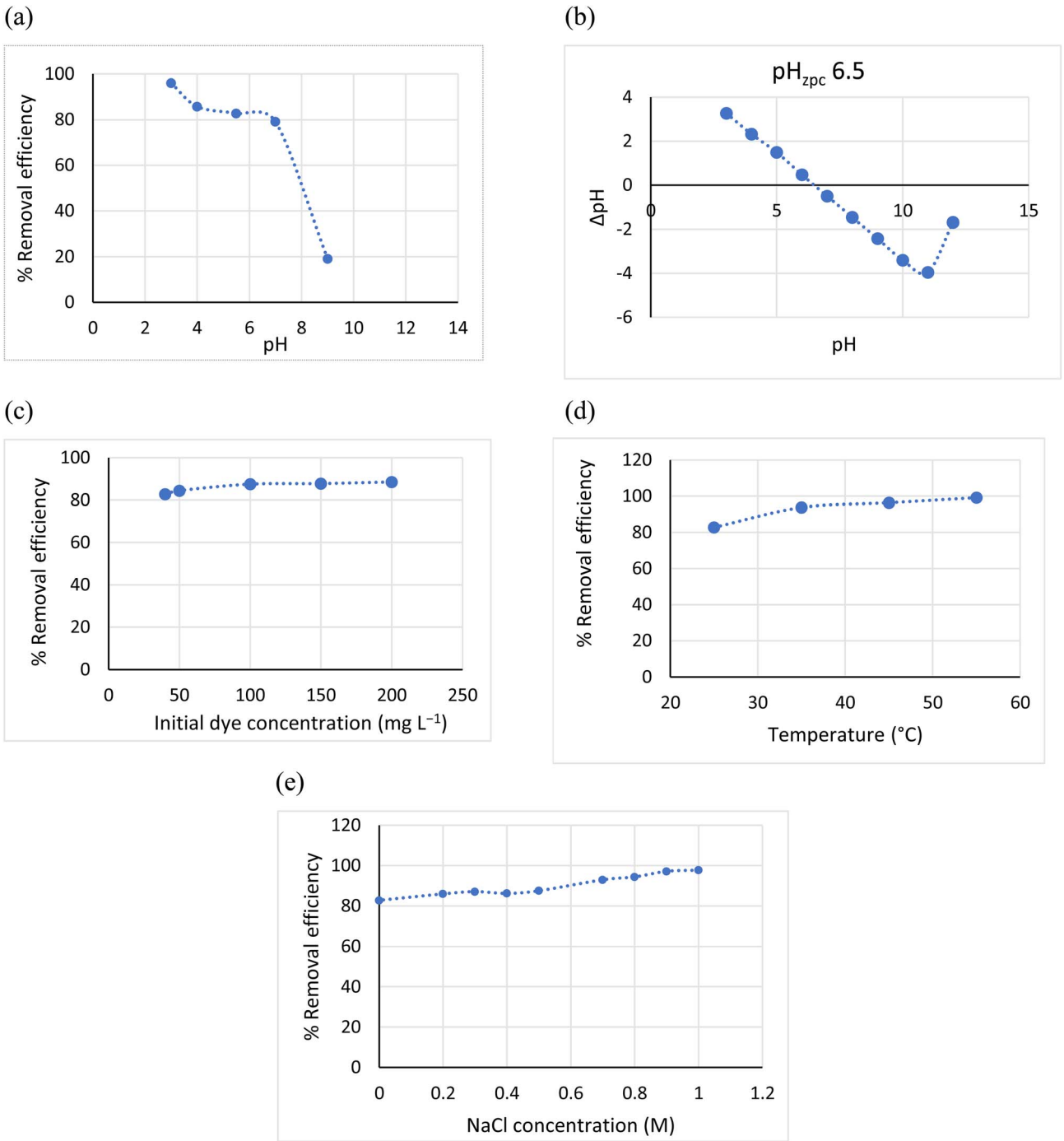

Fig. 7 Effect of various adsorption conditions; (a) solution pH, (b) pH_{zpc}, (c) initial dye concentration, (d) temperature, and (e) ionic strength on the removal efficiency of CR dye using His–Cs.

positively charged, promoting the uptake of negatively charged ions. In this study, the pH_{zpc} of His–Cs was determined to be 6.5 using the salt addition method as shown in Fig. 7(b). Accordingly, the His–Cs surface becomes increasingly protonated as the pH decreases, leading to surface cationization. This behavior is attributed to the presence of protonated functional groups such as $-NH^+$, $-NH_2^+$, $C{=}OH^+$, $-OH_2^+$, and $-NH_3^+$.[48,49] Further, the His–Cs possesses several heteroatoms, oxygen and nitrogen, thus it cannot be ruled out the binding between the CR dye and the His–Cs *via* hydrogen bonding.[22] The π–π stacking attractive forces between aromatic nuclei of both the CR dye and the His–Cs adsorbent aren't also ruled out. Therefore, the probable mechanism comprises a conjunction of His–Cs–CR dye electrostatic interaction, *via* the positively charged protonated groups on His–Cs and the negatively charged CR dye ions, in addition to H-bonding and π–π stacking interactions.[40]

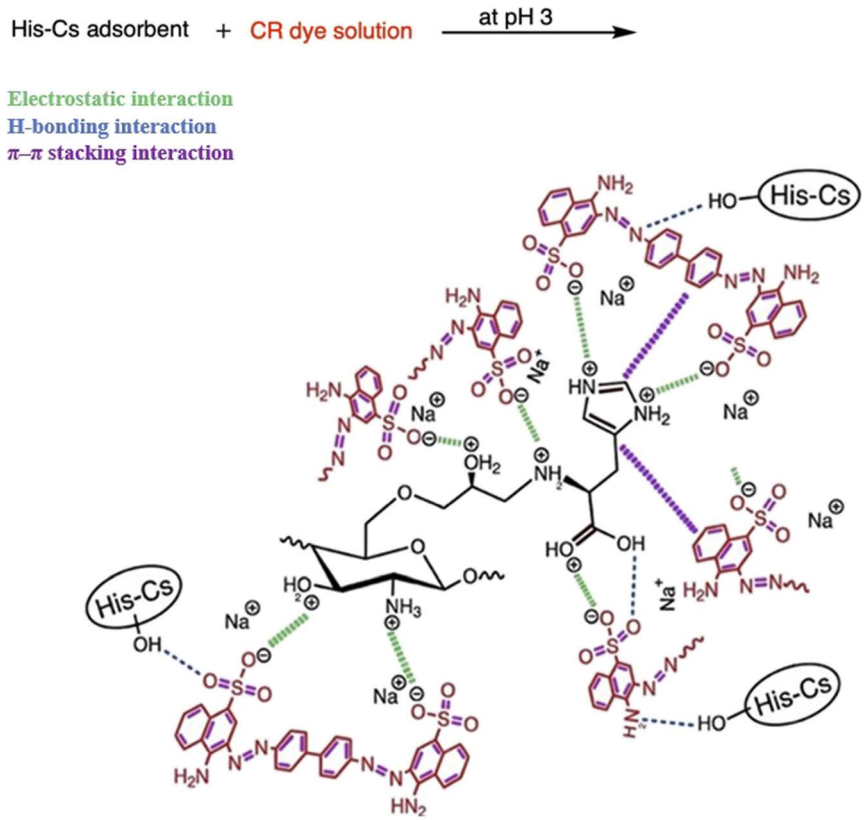

Scheme 2 Schematic illustration of the interaction of CR dye with His–Cs adsorbent at pH 3.

However, the electrostatic interaction may be the prime mechanism for the removal behavior (Scheme 2).

The effect of varying initial concentrations (40–200 ppm) of CR dye on adsorption was analyzed, as illustrated in Fig. 7(c). The adsorptive removal of CR dye increased from 82.78% to 88.54% as the concentration increased from 40 ppm to 200 ppm, probably a result of the saturation of adsorption sites when CR dye concentrations increase.

The data presented in Fig. 7(d) illustrates that the adsorptive removal of CR dye increased from 82.78% to 99.17% as the temperature rose from 25 to 55 °C. This trend indicates that the higher temperatures facilitate the adsorption process, suggesting an endothermic nature of the adsorption.

The ionic strength of the solution is a crucial factor influencing both electrostatic and non-electrostatic interactions between dye molecules and the adsorbent surface. To examine its impact on CR removal, different concentrations of NaCl were added to the dye solution. As illustrated in Fig. 7(e), the removal efficiency of CR increased markedly with rising salt concentration, reaching 97.73% compared to the initial 82.78% when the NaCl concentration was elevated from 0 to 1 M. This enhancement in adsorption performance can be attributed to the salting-out effect. At higher ionic strengths, Na^+ and Cl^- ions strongly associate with surrounding water molecules, reducing the availability of free water in the bulk solution. Consequently, the solubility of CR decreases because water molecules preferentially solvate the salt ions rather than the dye molecules. The reduced solubility promotes the transfer of CR dye from the aqueous phase to the surface of His–Cs. As a result, dye molecules are more likely to adsorb onto the His–Cs matrix instead of remaining dispersed in solution, leading to improved adsorption efficiency.[50–52]

3.5. Kinetics study

Adsorption kinetics are vital for evaluating the efficiency of the adsorption process. In this study, several kinetic models, including pseudo first order, pseudo second order, and Elovich were employed to investigate the adsorption behavior of CR dye onto His–Cs (Fig. 8). All kinetic parameters values obtained from the applied models are summarized in Table 3. The results in Table 3 clearly indicated that the adsorption of CR dye onto His–Cs followed the Elovich model, demonstrating superior fitting and exhibiting a high value of correlation coefficient ($R^2 \geq 0.999$) and low X^2.

3.6. Adsorption isotherms

To understand how CR dye is adsorbed onto His–Cs adsorbent and to establish the equilibrium data, the quantities of adsorbed material and the residual CR dye in the solution was analyzed using the Langmuir, Freundlich, and Temkin isotherm models (Fig. 9). Table 4 presents the comparative values of several parameters derived from these isotherm models. The correlation coefficient results indicate that the adsorption of CR dye on His–Cs aligns more closely with the

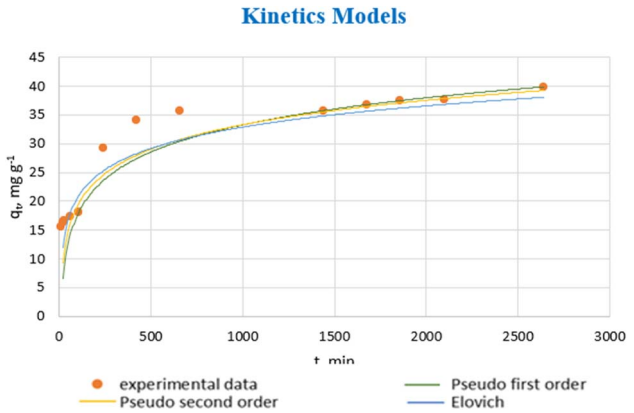

Fig. 8 Kinetic curves of pseudo-first-order, pseudo-second-order, and Elovich models (initial dye concentration = 40 ppm, temp. = 25 °C, pH = 5.5, volume of dye solution = 100 mL, His–Cs dose = 100 mg).

Table 3 Kinetic model constants and correlation coefficients for the adsorption of CR dye using His–Cs

Kinetic model	Parameter	Value
Pseudo-first-order	k_1 (min^{-1})	0.013
	$q_{e,\,cal.}$ (mg g^{-1})	35.804
	$q_{e,\,exp.}$ (mg g^{-1})	39.75
	R^2	0.995
	X^2	47.889
Pseudo-second-order	k_2 (g mg^{-1} min^{-1})	0.0006
	$q_{e,\,cal.}$ (mg g^{-1})	37.39
	R^2	0.998
	X^2	19.322
Elovich	α (mg g^{-1} min^{-1})	5.292
	β (g mg^{-1})	0.200
	R^2	0.999
	X^2	3.993

Temkin model, suggesting that the heat of adsorption changes linearly with the extent of surface coverage.

3.7. Thermodynamic study

Thermodynamic analysis of the solid–liquid adsorption of CR dye onto His–Cs was performed to elucidate the adsorption mechanism. The calculated thermodynamic parameters at 298, 308, 318, and 328 K are summarized in Table 5. The Gibbs free energy change (ΔG°) was employed to evaluate the spontaneity of the adsorption process. The negative ΔG° values obtained at all investigated temperatures indicate that CR adsorption onto His–Cs occurs spontaneously. These results confirm both the thermodynamic feasibility and favorable nature of the adsorption process within the studied temperature range. Furthermore, Table 5 reveals that ΔG° becomes more negative with increasing temperature, suggesting that adsorption is enhanced at elevated temperatures. The increased favorability of adsorption from 298 to 328 K can be attributed to improved mobility of CR dye molecules in solution at higher temperatures, which facilitates their interaction with active sites on the His–Cs surface.

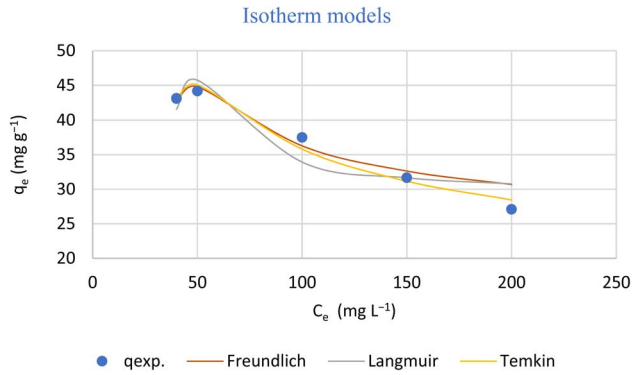

Fig. 9 Adsorption isotherm models of Langmuir, Frendlich, and Temkin (time = 48 h, temperature = 25 °C, pH = 5.5, volume of dye solution = 10 mL, His–Cs dose = 10 mg).

Table 4 Isotherm model constants and correlation coefficients for the adsorption of CR dye using His–Cs

Isotherm model	Parameter	Value
Langmuir	K_L (mg g^{-1})	−0.434
	q_{max} (mg g^{-1})	27.681
	R_L	(−0.061) – (−0.012)
	R^2	1
	X^2	31.152
Freundlich	K_F (mg g^{-1})	72.882
	$1/n$	−3.620
	R^2	0.821
	X^2	2.925
Temkin	B	−12.135
	K_T (L g^{-1})	0.004
	R^2	1
	X^2	5.791

Table 5 Thermodynamic study for the sorption of CR dye onto His–Cs

Temperature (K)	ΔG° (kJ mol^{-1})	ΔS° (J mol^{-1} K^{-1})	ΔH° (kJ mol^{-1})
298	−3.890	0.290	82.692
308	−6.935		
318	−8.683		
328	−13.033		

In this study, the thermodynamic parameter enthalpy (ΔH°) was calculated to elucidate the nature of CR dye adsorption onto the His–Cs adsorbent. The positive ΔH° value indicate that the adsorption process is endothermic. This behavior suggests that during adsorption, the CR dye molecules likely replace more than one pre-adsorbed water molecule on the His–Cs surface, thereby contributing to the observed endothermic character. Solid–liquid adsorption generally involves two simultaneous steps: the desorption of solvent molecules (commonly water) initially bound to the adsorbent surface, followed by the attachment of the adsorbate species. In an exothermic adsorption process, the energy required to break existing bonds is

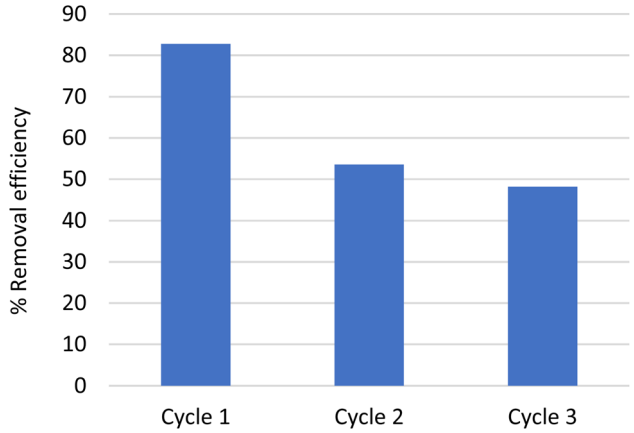

Fig. 10 Recyclability performance of His–Cs over three consecutive of the adsorption cycles of CR dye molecules.

lower than the energy released upon formation of new adsorbate–adsorbent interactions, resulting in net heat evolution. Furthermore, as reported by Saha and Chowdhury,[53] the magnitude of the enthalpy change provides insight into the adsorption mechanism. Physical adsorption typically exhibits enthalpy values comparable to the heat of condensation (2.1–20.9 kJ mol^{-1}), whereas chemisorption is characterized by significantly higher values, ranging from 80 to 200 kJ mol^{-1}. Based on the ΔH° values summarized in Table 5, the adsorption of CR dye onto His–Cs can therefore be categorized as a chemisorption process.

In the present investigation, the entropy change (ΔS°) was calculated to assess the affinity of His–Cs toward CR dye molecules. As reported by Saha and Chowdhury,[53] positive entropy values indicate increased randomness at the solid–liquid interface, often accompanied by structural rearrangements in both the adsorbate and the adsorbent. The positive ΔS° value obtained in this study therefore reflect a strong affinity of His–Cs for CR. Furthermore, the positive entropy change observed in the single-component adsorption system suggests that CR dye molecules replace water molecules previously adsorbed on the His–Cs surface. The release of these water molecules into the bulk solution increases their translational freedom, resulting in a net gain in entropy that exceeds any entropy loss associated with CR dye adsorption. Consequently, the overall process is characterized by enhanced disorder within the system.

3.8. Reusability study

For practical implementation of continuous sorption systems, adsorbent reusability is a critical parameter. The regeneration capability of an adsorbent significantly influences the economic viability of adsorption-based water treatment processes. In this study, the recyclability of His–Cs was evaluated through successive adsorption–desorption cycles, and the percentage decolorization achieved in each cycle was determined (Fig. 10). The results demonstrated a gradual decrease in decolorization efficiency with increasing cycle number, which may be attributed to incomplete desorption of retained dye molecules from the adsorbent surface. Nevertheless, the removal efficiency of CR dye remained above 48% after three consecutive cycles. These findings confirm that His–Cs possesses acceptable reusability and retains considerable adsorption performance after repeated use.[22]

3.9. Analysis of sorption capacity for CR dye on different adsorbents

This study compares the adsorption capacities of the His–Cs for the CR dye with those of the other adsorbents, as presented in Table 6. The His–Cs adsorbent demonstrated a superior

Table 6 Assessment of the adsorption capabilities of different adsorbents for the removal of CR dye

Adsorbents	Adsorption capacity, q_{max} (mg g^{-1})	pH	Initial dye concentration (ppm)	Dosage of adsorbent (g L^{-1})	References
Zeolite (clay materials)	3.77	7.5 ± 0.3	150.0	100.0	54
ZrO_2 reagent	4.8 ± 0.2	7.0	35.0	0.4	55
Natural kaolin (K)	5.94	6.9	100.0	10.0	56
Australian kaolin clay K15GR	6.81	7.5 ± 0.3	200.0	50.0	57
Australian kaolin clay Ceram	7.27	7.5 ± 0.3	250.0	20.0	57
Nickel oxide nanoparticles	10.1	5.0	20.0	0.5	58
Montmorillonite	12.70	7.0	100.0	4.0	59
H_{13}	13.78	7	18.0	1.0	40
H_{11}	16.247	7	18.0	1.0	40
H_{31}	17.93	7	18.0	1.0	40
H_{31}/AgNPs 5%	17.98	7	18.0	1.0	40
Polypyrrole	18.0	3.0	40.0	2.0	60
Raw rectorite (R-REC)	19.50	7.0	500.0	1.0	61
ZrO_2 solid spheres	21.4 ± 1.1	7.0	35.0	0.4	55
Open burnt clay	22.86	3.0	50.0	2.5	62
Cetyltrimethylammonium bromide-modified kaolin (CTAB-kaolin or KC)	24.46	6.9	100.0	10.0	56
Raw clay	27.03	7.5 ± 0.2	50.0	10.0	38
His–Cs	39.67	5.5	40.0	1.0	This study

adsorption capacity for CR dye compared to several reported adsorbents,[40,54–62] as detailed in Table 6. This indicates the potential for enhancing the adsorption capacity of Cs for CR dye through its combination with His. This results from the integration of various cationized functional groups that serve as binding sites for the anionic CR dye. In conclusion, the synthesized His–Cs is deemed a favorable adsorbent for CR dye removal.

4. Conclusion

His–Cs, intended for the adsorption of CR dye from aqueous solution, was produced using a two-step process; initially, His interacted with epichlorohydrin in an alkaline medium, followed by the interaction of the resultant product with Cs in the same medium. Comprehensive characterization employing FTIR, XRD, SEM, and EDS techniques was conducted to validate the chemical structure of the synthesized material. The adsorption kinetics of CR dye onto His–Cs conformed predominantly to the Elovich model, while the Temkin isotherm model provided an excellent fit to the experimental equilibrium data, suggesting that the heat of adsorption changes linearly with the extent of surface coverage. The CR dye adsorption onto His–Cs occurs spontaneously, confirming the feasibility and favorable nature of the adsorption process. The adsorption process is endothermic, indicating a chemisorption process. His–Cs possesses acceptable reusability and retains considerable adsorption performance after repeated use. Collectively, these results substantiate that His–Cs behaves as a highly effective adsorbent for the elimination of CR dye from aqueous media.

Author contributions

J. S. A., N. F. A., A. A., T. A. and N. A. M. performed the experimental part, prepared all figures, interpreted the data, carried out the analysis and wrote the main manuscript text, revised the manuscript and helped in manuscript correction. N. A. M. conceptualized and conceived the research work, supervised all steps of the research, interpreted and discussed the experimental data, wrote, reviewed and edited the manuscript. All authors read and approved the final manuscript.

Conflicts of interest

There are no conflicts to declare.

Data availability

Data available within the article.

Acknowledgements

The Researchers would like to thank the Deanship of Graduate Studies and Scientific Research at Qassim University for financial support (QU-APC-2026).

References

1 F. W. Owa, Water pollution: sources, effects, control and management, *Int. Lett. Nat. Sci.*, 2014, **8**, 1–6.
2 M. Necibi and N. Mzoughi, Chapter 1: the distribution of organic and inorganic pollutants in marine environment, in *Micropollutants: Sources, Ecotoxicological Effects and Control Strategies*, ed. N. Tabitha, Nova Science Publishers, Inc., London, UK, 2017, pp. 1–44.
3 N. A. Mohamed, N. F. Al-Harby and M. S. Almarshed, Effective removal of Basic Red 12 dye by novel antimicrobial trimellitic anhydride isothiocyanate-cross-linked chitosan hydrogels, *Polym. Polym. Compos.*, 2021, **29**, S274–S287.
4 Z. Millbern, A. Trettin, R. Wu, M. Demmler and N. R. Vinueza, Synthetic dyes: a mass spectrometry approach and applications, *Mass Spectrom. Rev.*, 2024, **43**, 327–344.
5 L. Lin, H. Yang and X. Xu, Effects of water pollution on human health and disease heterogeneity: a review, *Front. Environ. Sci.*, 2022, **10**, 880246.
6 R. AlTohamy, S. S. Ali, F. Li, K. M. Okasha, Y. A. G. Mahmoud, T. Elsamahy, H. Jiao, Y. Fu and J. Sun, A critical review on the treatment of dye-containing wastewater: ecotoxicological and health concerns of textile dyes and possible remediation approaches for environmental safety, *Ecotoxicol. Environ. Saf.*, 2022, **231**, 113160.
7 E. F. Albahly, N. F. Al-Harby, H. N. Alqifari, T. Kernane and N. A. Mohamed, Efficient adsorption of fast green dye by chitosan modified with cyanoguanidine: statistical modelling, kinetic, and isotherm studies, *BMC Chem.*, 2026, **20**, 92.
8 K. T. Chung, Azo dyes and human health: a review, *J. Environ. Sci. Health, Part C:Environ. Carcinog. Ecotoxicol. Rev.*, 2016, **34**, 233–261.
9 C. V. Rao, Benzidine, Reference Module in Biomedical Sciences, *Encyclopedia of Toxicology*, 3rd edn, 2014, pp. 419–422.
10 P. O. Oladoye, M. O. Bamigboye, O. D. Ogunbiyi and M. T. Akano, Toxicity and decontamination strategies of Congo red dye, *Groundw. Sustain. Dev.*, 2022, **19**, 100844.
11 S. I. Siddiqui, E. S. Allehyani, S. A. Al-Harbi, Z. Hasan, M. A. Abomuti, H. K. Rajor and S. Oh, Investigation of Congo red toxicity towards different living organisms: a review, *Processes*, 2023, **11**, 807.
12 E. S. Mansor, H. Abdallah and A. M. Shaban, Highly effective ultrafiltration membranes based on plastic waste for dye removal from water, *Water Environ. Res.*, 2024, **96**, e11018.
13 K. Saini, A. Sahoo, J. Kumar, A. Kumari, K. K. Pant, A. Bhatnagar and T. Bhaskar, Effective utilization of discarded reverse osmosis post-carbon for adsorption of dyes from wastewater, *Environ. Res.*, 2023, **231**(2), 116165.
14 P. Gharbani, S. M. Tabatabaii and A. Mehrizad, Removal of Congo red from textile wastewater by ozonation, *Int. J. Environ. Sci. Technol.*, 2008, **5**, 495–500.

15 D. Mansour, E. Alblawi, A. K. D. Alsukaibi and B. Al Shammari, Removal of Congo red dye by electrochemical advanced oxidation process: optimization, degradation pathways, and mineralization, *Sustain. Water Resour. Manag.*, 2024, **10**, 4.
16 S. Goudjil, S. Guergazi, T. Masmoudi and S. Achour, Effect of reactional parameters on the elimination of Congo red by the combination of coagulation–floculation with aluminum sulfate, *Desalin. Water Treat.*, 2021, **209**, 429–436.
17 M. I. Khan, S. Akhtar, S. Zafar, A. Shaheen, M. A. Khan, R. Luque and A. U. Rehman, Removal of Congo red from aqueous solution by anion exchange membrane (EBTAC): adsorption kinetics and thermodynamics, *Materials*, 2015, **8**, 4147–4161.
18 S. Khan, T. Noor, N. Iqbal and L. Yaqoob, Photocatalytic dye degradation from textile wastewater: a review, *ACS Omega*, 2024, **9**, 21751–21767.
19 S. Almotiry, D. M. S. Almuthaybiri, N. F. Al-Harby and N. A. Mohamed, Adsorption of ciprofloxacin onto CMCs/XG hydrogel: optimization, kinetic, and isotherm studies, *Polymers*, 2026, **18**, 632.
20 B. A. Alimi, S. Pathania, J. Wilson, B. Duffy and J. M. C. Fria, Extraction, quantification, characterization, and application in food packaging of chitin and chitosan from mushrooms: a review, *Int. J. Biol. Macromol.*, 2023, **237**, 124195.
21 I. Aranaz, A. R. Alcántara, M. C. Civera, C. Arias, B. Elorza, C. A. Heras and N. Acosta, Chitosan: an overview of its properties and applications, *Polymers*, 2021, **13**, 3256.
22 N. F. Al-Harby, E. F. Albahly and N. A. Mohamed, Synthesis and characterization of novel uracil-modified chitosan as a promising adsorbent for efficient removal of Congo red dye, *Polymers*, 2022, **14**, 271.
23 V. K. Konaganti, R. Kota, S. Patil and G. Madras, Adsorption of anionic dyes on chitosan grafted poly(alkyl methacrylate) s, *Chem. Eng. J.*, 2010, **158**, 393–401.
24 B. F. Far, M. R. Naimi-Jamal, M. Jahanbakhshi, S. A. Khalafvandi, M. Alian and D. R. Jahromi, Decontamination of Congo red dye from aqueous solution using nanoclay/chitosan-graft-gelatin nanocomposite hydrogel, *J. Mol. Liq.*, 2024, **395**, 123839.
25 R. T. Alfuraydi, N. F. Al-Harby, F. M. Alminderej, N. Y. Elmehbad and N. A. Mohamed, Poly (vinyl alcohol) hydrogels boosted with cross-linked chitosan and silver nanoparticles for efficient adsorption of Congo red and Crystal violet dyes, *Gels*, 2023, **9**, 882.
26 L. You, C. Huang, F. Lu, A. Wang, X. Liu and Q. Zhang, Facile synthesis of high performance porous magnetic chitosan - polyethylenimine polymer composite for Congo red removal, *Int. J. Biol. Macromol.*, 2018, **107**, 1620–1628.
27 N. A. Mohamed, N. F. Al-Harby and M. S. Almarshed, Enhancement of adsorption of Congo red dye onto novel antimicrobial trimellitic anhydride isothiocyanate-cross-linked chitosan hydrogels, *Polym. Bull.*, 2020, **77**, 6135–6160.
28 R. A. Alharbi, F. M. Alminderej, N. F. Al-Harby, N. Y. Elmehbad and N. A. Mohamed, Preparation and characterization of a new bis-uracil chitosan-based hydrogel as efficient adsorbent for removal of anionic Congo red dye, *Polymers*, 2023, **15**, 1529.
29 N. F. Al-Harby, R. S. Almutairi, N. Y. Elmehbad and N. A. Mohamed, A novel O-carboxymethyl chitosan-based hydrogel of an outstanding adsorption performance for removal of cationic Basic red 12 dye from its aqueous solution, *Polym. Eng. Sci.*, 2023, **63**, 2336–2353.
30 M. M. Beppua, E. J. Arruda, R. S. Vieira and N. N. Santos, Adsorption of Cu(II) on porous chitosan membranes functionalized with histidine, *J. Membr. Sci.*, 2004, **240**, 227–235.
31 A. Eser, V. N. Tirtom, T. Aydemir, S. Becerik and A. Dinçer, Removal of nickel(II) ions by histidine modified chitosan beads, *Chem. Eng. J.*, 2012, **210**, 590–596.
32 M. T. Maia, D. N. Sena, G. B. Calais, F. M. T. Luna, M. M. Beppu and R. S. Vieira, Effects of histidine modification of chitosan microparticles on metal ion adsorption, *React. Funct. Polym.*, 2020, **154**, 104694.
33 T. B. Taketa, C. R. A. Mahl, G. B. Calais and M. M. Beppu, Amino acid-functionalized chitosan beads for in vitro copper ions uptake in the presence of histidine, *Int. J. Biol. Macromol.*, 2021, **188**, 421–431.
34 K.-L. Chang, Y. Higuchi, S. Kawakami, F. Yamashita and M. Hashida, Efficient gene transfection by histidine-modified chitosan through enhancement of endosomal escape, *Bioconjug. Chem.*, 2010, **21**, 1087–1095.
35 S. Abbad, Z. Zhang, A. Y. Waddad, W. L. L. Munyendo, H. Lv and J. Zhou, Chitosan-modified cationic amino acid nanoparticles as a novel oral delivery system for insulin, *J. Biomed. Nanotechnol.*, 2014, **10**, 1–14.
36 D. George, P. U. Maheswari and K. M. M. S. Begum, Chitosan-cellulose hydrogel conjugated with L-histidine and zinc oxide nanoparticles for sustained drug delivery: kinetics and in-vitro biological studies, *Carbohydr. Polym.*, 2020, **236**, 116101.
37 M. A. Raja, M. Arif, C. Feng, S. Zeenat and C.-G. Liu, Synthesis and evaluation of pH-sensitive, self-assembled chitosan-based nanoparticles as efficient doxorubicin carriers, *J. Biomater. Appl.*, 2017, **31**, 1182–1195.
38 A. Ghribi, M. Bagane and M. Chlendi, Sorptive removal of congo red from aqueous solutions using raw clay: batch and dynamic studies, *Int. J. Innov. Environ. Stud. Res.*, 2014, **2**, 45–56.
39 A. e. M. E. Mohammed, N. F. Al-Harby, M. Alrasheedi, S. M. Ibrahim and N. A. Mohamed, Cyanoguanidine-modified chitosan as an efficacious adsorbent for removing cupric ions from aquatic solutions: kinetics, isotherms, and mechanisms, *Inorganics*, 2025, **13**, 116.
40 N. F. Al-Harby, E. F. Albahly and N. A. Mohamed, Kinetics, isotherm and thermodynamic studies for efficient adsorption of Congo Red dye from aqueous solution onto novel cyanoguanidine-modified chitosan adsorbent, *Polymers*, 2021, **13**, 4446.
41 N. F. Al-Harby, R. S. Almutairi and N. A. Mohamed, Adsorption behavior of methylene blue dye by novel crosslinked O-CM-chitosan hydrogel in aqueous solution:

kinetics, isotherm and thermodynamics, *Polymers*, 2021, **13**, 3659.

42 K. H. Chu, Revisiting the Temkin isotherm: dimensional inconsistency and approximate forms, *Ind. Eng. Chem. Res.*, 2021, **60**, 13140–13147.

43 G. Kalaba, J. Nyirenda and O. Munyati, Characterisation of activated carbons for removal of organic and heavy metal pollutants from water in resource limited countries, *Desalination Water Treat.*, 2022, **261**, 224–233.

44 N. F. Al-Harby, M. Alrasheedi, A. e. M. E. Mohammed, S. M. A. Soliman and N. A. Mohamed, Effective removal of Cu(II) ions from aqueous solution by cross-linked chitosan-based hydrogels, *Water*, 2024, **16**, 2324.

45 R. T. Alfuraydi, F. M. Alminderej and N. A. Mohamed, Evaluation of antimicrobial and anti-biofilm formation activities of novel poly (vinyl alcohol) hydrogels reinforced with crosslinked chitosan and silver nano-particles, *Polymers*, 2022, **14**, 1619.

46 N. Y. Elmehbad, N. A. Mohamed and N. A. Abd El-Ghany, Evaluation of the antimicrobial and anti-biofilm activity of novel salicylhydrazide chitosan derivatives impregnated with titanium dioxide nanoparticles, *Int. J. Biol. Macromol.*, 2022, **205**, 719–730.

47 M. Alrasheedi, A. e. M. E. Mohammed, N. F. Al-harby, G. E. Khedr and N. A. Mohamed, Adsorptive elimination of Cu(II) ions from aqueous solution onto chitosan modified with uracil, *Water*, 2024, **16**, 3695.

48 U. Yunusa, B. Usman and M. B. Ibrahim, Adsorptive removal of Basic dyes and hexavalent chromium from synthetic industrial effluent: adsorbent screening, kinetic and thermodynamic studies, *Int. J. Eng. Manuf.*, 2020, **10**, 54–74.

49 K. Shukla, A. Verma, L. Verma, S. Rawat and J. Singh, A novel approach to utilize used disposable Paper cups for the development of adsorbent and Its application for the Malachite Green and Rhodamine-B dyes removal from aqueous solutions, *Nat. Environ. Pollut. Technol.*, 2020, **19**, 57–70.

50 M. Cetina, P. Mihovilović, A. Pešić and B. Vojnović, Influence of ionic strength and temperature on the adsorption of Reactive Black 5 dye by activated carbon: kinetics, mechanisms and thermodynamics, *Molecules*, 2025, **30**, 2593.

51 K. R. Shoueir, Green microwave synthesis of functionalized chitosan with robust adsorption capacities for Cr (VI) and/or RHB in complex aqueous solutions, *Environ. Sci. Pollut. Res.*, 2020, **27**, 33020–33031.

52 B. Chen, H. Zhao, S. Chen, F. Long, B. Huang, B. Yang and X. Pan, A magnetically recyclable chitosan composite adsorbent functionalized with EDTA for simultaneous capture of anionic dye and heavy metals in complex wastewater, *Chem. Eng. J.*, 2019, **356**, 69–80.

53 P. Saha and S. Chowdhury, Insight into adsorption thermodynamics, *Thermodynamics*, 2011, **16**, 349–364.

54 H. Hu, J. Liu, Z. Xu, L. Zhang, B. Cheng and W. Ho, Hierarchical porous Ni/Co-LDH hollow dodecahedron with excellent adsorption property for Congo red and Cr(VI) ions, *Appl. Surf. Sci.*, 2019, **478**, 981–990.

55 C. Wang, Y. Le and B. Cheng, Fabrication of porous ZrO2 hollow sphere and its adsorption performance to Congo red in water, *Ceram. Int.*, 2014, **40**(part B), 10847–10856.

56 M. A. Zenasni, B. Meroufel, A. Merlin and B. George, Adsorption of Congo Red from Aqueous Solution Using CTAB-Kaolin from Bechar Algeria, *J. Surf. Eng. Mater. Adv. Technol.*, 2014, **4**, 332–341.

57 V. Vimonses, S. Lei, B. Jin, C. W. K. Chow and C. Saint, Adsorption of congo red by three Australian kaolins, *Appl. Clay Sci.*, 2009, **43**, 465–472.

58 F. Falaki and A. Fakhri, Adsorption properties of nickel oxide nanoparticles for removal of Congo Red from aqueous solution, *J. Phys. Theor. Chem.*, 2014, **10**, 255–262.

59 L. Wang and A. Wang, Adsorption characteristics of Congo Red onto the chitosan/montmorillonite nanocomposite, *J. Hazard. Mater.*, 2007, **147**, 979–985.

60 S. Karthikaikumar, M. Karthikeyan and K. K. S. Kumar, Removal of Congo Red Dye from Aqueous Solution by Polyani-line-Montmorrillonite Composite, *Chem. Sci. Rev. Lett.*, 2014, **2**, 606–614.

61 Y. Liu, W. Wang and A. Wang, Removal of congo red from aqueous solution by sorption on organified rectorite, *Clean:Soil, Air, Water*, 2010, **38**, 670–677.

62 M. A. Mumin, M. M. R. Khan, K. F. Akhter and M. J. Uddin, Potentiality of open burnt clay as an adsorbent for the removal of Congo red from aqueous solution, *Int. J. Environ. Sci. Technol.*, 2007, **4**, 525–532.